Influence of carbon on the kinetics of He migration and clustering in α-Fe from first principles

C. J. Ortiz,[1,*] M. J. Caturla,[2] C. C. Fu,[3,†] and F. Willaime[3]
[1]*Laboratorio Nacional de Fusión por Confinamiento Magnético, CIEMAT, 28040 Madrid, Spain*
[2]*Departamento de Física Aplicada, Universidad de Alicante, 03690 San Vicente del Raspeig, Spain*
[3]*CEA, DEN, Service de Recherches de Métallurgie Physique, F-91191 Gif-sur-Yvette, France*
(Received 14 May 2009; revised manuscript received 4 August 2009; published 8 October 2009)

Density functional theory (DFT) calculations have been performed to study the interaction of carbon with He-vacancy complexes in α-Fe. Using the DFT predictions, a rate theory model that accounts for the evolution of carbon, helium, and defects created during irradiation has been developed to explore the influence of carbon on the kinetics of He diffusion and clustering after implantation in α-Fe. This DFT-based rate theory model predicts that carbon not only influences vacancy (V) migration but also He desorption, enhancing He mobility in particular for low V/C ratios. The reason for this behavior is mainly the formation of VC and VC_2 complexes, which significantly reduces the mobility of vacancies with respect to pure Fe, inhibiting the formation of higher order clusters, i.e., He_nV_m, and increasing thus the number of He at substitutional positions at room temperature. Assuming reasonable values of carbon concentration, we successfully reproduce and interpret existing desorption experimental results, where all the energetic parameters for the relevant reactions were obtained from first-principles calculations. In addition, our study provides a detailed explanation of the various He migration mechanisms that prevail under the considered experimental conditions.

DOI: 10.1103/PhysRevB.80.134109 PACS number(s): 61.80.Az, 61.72.Cc, 61.72.J−, 66.30.−h

I. INTRODUCTION

The development of advanced radiation resistant materials requires fundamental knowledge about defect production, their diffusion, and clustering. In the case of structural materials for future fusion devices, the effect of helium on defect evolution and its consequences on material properties is of particular interest[1] since it is well known that helium induces void swelling. Ferritic/martensitic steels have been proposed as candidate materials for fusion devices partly due to their low swelling rates.[2] However, these steels suffer from embrittlement and the role of He on this detrimental phenomena is still not well understood.[3] Predicting the fate of He in α-Fe is thus crucial for the development of advanced ferritic materials resistant to radiation under fusion and fission conditions.

During the past decade much fundamental knowledge has been gained about defects in α-Fe through both basic experiments and first-principles simulations. For instance, *ab initio* calculations have revealed that the magnetic character of α-Fe plays a significant role in the behavior of those defects produced by irradiation.[4–6] Accurate migration energies of elementary defects in this material have also been obtained by these calculation methods.[7] First-principles predictions can then be used in kinetic models such as kinetic Monte Carlo, as in Ref. 7, or rate theory (RT) to study the long-term evolution of defects produced by irradiation.[8]

However, when comparing simulation of defect evolution to experimental results one must take into account the presence of impurities and their possible interaction with point defects. This is the case of α-Fe where carbon is always present. In fact, only a small number of experiments have been performed using ultrahigh purity Fe (Ref. 9) with carbon levels below the detection limit, i.e., about 5 atomic part per million (at.ppm). When present in sufficient concentration, carbon is known to affect the migration of self-defects in α-Fe, particularly vacancies. Early experiments[9,10] showed that both electrical resistivity and positron lifetime of electron irradiated α-Fe change significantly with carbon content. New annealing stages were associated to the formation of various carbon-defect complexes, in particular C-vacancy complexes.[9] Other authors[11,12] have also pointed out that the effective migration energy of vacancies in α-Fe measured experimentally varies between 0.6 and 1.5 eV with higher values for specimens with higher carbon content. Some of these observations have been recently explained with the help of density functional theory (DFT) calculations.[13–16] These studies show that there is a high binding energy between carbon at interstitial sites and vacancies, which results in a slower diffusion for vacancies in α-Fe containing carbon, with respect to that observed in pure Fe.

On the other hand, we have recently shown[17] that in order to reproduce measured He desorption data[18] obtained from irradiated Fe, a rather high effective value for the migration energy of vacancies must be used. We attributed this value to an impurity effect with carbon being the most likely candidate. Furthermore, according to these calculations, this impurity should also have an effect on the stability of He-vacancy complexes. A first model including carbon impurities and their effect on He kinetics was made in Ref. 19. This models includes only two types of carbon clusters, namely, VC and HeVC. A good agreement with experimental data could be obtained with this simplified model by modifying the binding energies of VC and HeVC clusters.

In this paper we propose a DFT-based RT model that accounts for the evolution of helium in irradiated α-Fe containing carbon. We want to emphasize that in contrast to our previous works,[17,19] the model presented here takes explicitly into account the presence of carbon and its possible interactions with He-V clusters. The proposed model follows thus the evolution of self-interstitials, vacancies, helium, carbon, He-V-C complexes, and the formation of defect clusters in irradiated α-Fe. All migration and binding energies of de-

fects taken into account in the kinetic model were obtained by means of DFT calculations, which are presented in Sec. II. Section III describes the different atomistic mechanisms included in the model as well as the rate equations used to predict He diffusion and clustering in α-Fe. In Sec. IV this model is applied to study the mechanisms of He desorption in implanted Fe for different V/C ratios. Finally, existing experimental He desorption data are reproduced using the present DFT-based RT approach and concluding remarks are drawn in Sec. VI.

II. PROPERTIES OF HE-*V*-C CLUSTERS: DFT CALCULATIONS

A. Method of calculation

We have performed calculations within the density functional theory and the generalized gradient approximation as implemented in the SIESTA code.[20] The calculations are spin polarized to account for the magnetism within a collinear approach. Core electrons are replaced by nonlocal norm-conserving pseudopotentials while valence electrons are described by linear combinations of numerical pseudoatomic orbitals. The pseudopotential and the basis set for Fe and He atoms are the same as in Ref. 21. The cutoff radius for the pseudopotential of C is set to 0.66 Å, and its basis set includes two strictly localized functions for the 2*s* states and six for the 2*p* states. The cut-off radii are 2.22 and 2.64 Å, respectively. Five functions for the 3*d* states are also included as polarized orbitals in order to increase angular flexibility. The charge density is represented on a regular 0.078 Å width grid in the real space. The present approach has been shown to successfully account for the properties of point defects in iron[5,7] as well as in Fe containing either helium[21] or carbon.[14]

Supercell calculations were performed to study defect properties using 128-atom cells with a $3\times3\times3$ shifted *k*-point grid. The Methfessel-Paxton broadening scheme with a 0.3 eV width was used. Calculated defect energies have been verified to be well converged with respect to this *k*-point grid. All these calculations were performed at constant pressure, i.e., the structures were optimized by relaxing both the atomic positions and the volume and shape of the supercell.[7,21] In practice, four different cells with the same number of crystallographic sites are used to calculate the binding energy of a defect: cells I and II contain, respectively, an isolated defect and the initial complex, and cell III contains the complex resulting from the reaction. The binding energy is obtained by adding the energies of cells I and II, and subtracting the energy of cell III and that of a perfect-crystal supercell (cell IV). With this convention, a positive binding energy indicates an attractive interaction between the reactants. In the present case, the binding energies of defects (vacancy, C or He atoms) to $He_nV_mC_p$ complexes are defined as the energy differences between the configuration where the defect is infinitely separated from the cluster and where it is added to the cluster.

B. DFT results

1. He-*V*, *V*-C, and He-C interactions

The lowest-energy configurations obtained from DFT calculations for small helium-vacancy and carbon-vacancy complexes (HeV, He_2V, HeV_2, He_2V_2, VC, VC_2, and V_2C_2) are represented in Fig. 1. He atoms prefer to occupy substitutional sites in α-iron [Fig. 1(a)] while the lowest-energy position of C is the tetrahedral interstitial site. It is now well known that C and both substitutional and interstitial He (He_{int}) attract vacancies,[13–15,21,22] such interactions being much stronger than those between a He or C atom and a self-interstitial atom.[9,23] The resulting configurations are, respectively, the following: the carbon atom remains close to an interstitial site rather than being centered on the vacancy site [Fig. 1(e)]; the helium atom is located mid way between two nearest-neighbor vacancies [Fig. 1(c)]; and a helium becomes substitutional [Fig. 1(a)]. It is worth mentioning that a He interstitial decays spontaneously to a first neighbor vacancy, becoming a He substitutional and gaining 2.3 eV in energy. In contrast, C atoms tend to only decorate vacancies [Figs. 1(e) and 1(f), VC_2 being the optimal configuration, that is, the addition of more than two C atoms per vacancy does not induce further gain of energy.[14] Positron lifetime measurements have indeed pointed out the existence of such small carbon-decorated vacancy clusters.[10] Divacancies are most stable at second nearest neighbor. This remains the case when one or two carbon atoms are added [Figs. 1(g) and 1(h) but in presence of one or two He atoms the nearest-neighbor configuration becomes more stable [Figs. 1(c) and 1(d).

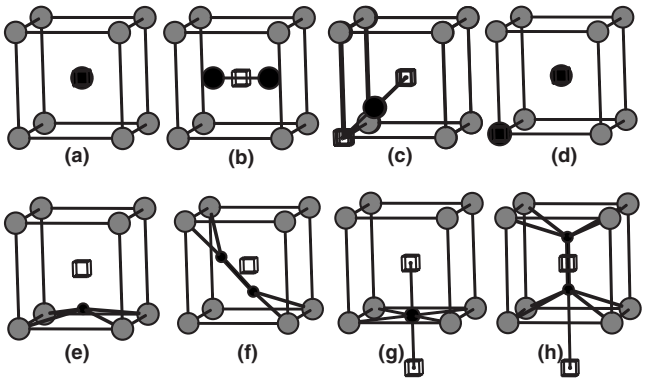

FIG. 1. Schematic representation of the lowest-energy configurations found from DFT calculations for: (a) HeV, (b) He_2V, (c) HeV_2, (d) He_2V_2, (e) VC, (f) VC_2, (g) V_2C, and (h) V_2C_2. The big and small black spheres denote He and C atoms, respectively, gray spheres are the neighboring Fe atoms, and the small empty cubes symbolize the vacancies. All the atoms are at their relaxed positions.

The interaction between C and a He interstitial is however repulsive for all interatomic distances smaller than $1.25a_0$ and practically vanishes beyond this distance, a_0 being the lattice parameter of bcc iron. This repulsion, similar to the C-C interaction,[13] is mainly related to a strong lattice distortion induced by the accumulation of interstitial solutes within a small interstitial volume. The situation is indeed different in presence of vacancies. He interstitial and C atoms attract each other close to vacancies forming stable ternary complexes. However, it is worth mentioning that there is any significant electronic hibridization between He and C in any situation. $He_nV_mC_p$ complexes with n, m, and $p=0$, 1 or 2 were considered in this study. In order to determine their lowest-energy configurations (Fig. 2), we have investigated

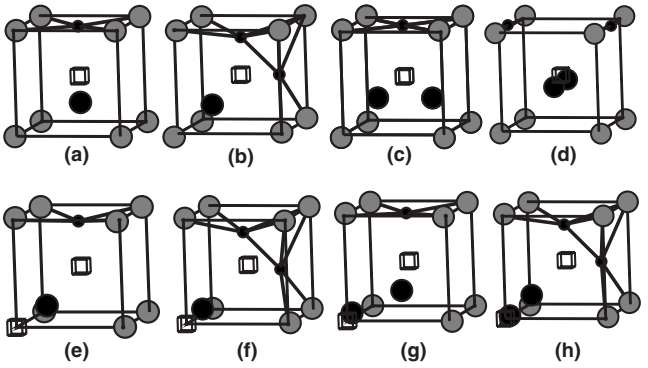

FIG. 2. Lowest-energy configurations found from DFT calculations for small $He_nV_mC_p$ complexes: (a) He*V*C, (b) HeVC_2, (c) He_2VC, (d) He_2VC_2, (e) HeV_2C, (f) HeV_2C_2, (g) He_2V_2C, and (h) $He_2V_2C_2$. The big and small black spheres denote the He and C atoms, respectively, gray spheres are the neighboring Fe atoms, and the small empty cubes symbolize the vacancies. All the atoms are at their relaxed positions.

up to ten structures for each ternary complex, based on possible combinations of the corresponding most stable He-vacancy and C-vacancy clusters configurations [Figs. 1(a)–1(h)].

Some characteristics of the lowest-energy structures that were found for $He_nV_mC_p$ complexes are interesting to be pointed out. Although He atoms prefer to be substitutional, they may sit on off-site positions in presence of C, as far as possible from the C atoms, which is a direct consequence of He-C repulsion. When there are two He atoms within a cluster, they tend to form a He-He ⟨100⟩ dumbbell, even though the He-He distance becomes longer than that in He_2V due to the presence of C. On the other hand, carbon atoms always stay at near-octahedral positions decorating the vacancies. When comparing Figs. 1 and 2 we see that C positions remain practically the same in clusters with and without He, except for He_2VC_2 and $He_2V_2C_2$ complexes. In the former cluster, the presence of two He atoms close to the vacancy inhibits the formation of the C dimer, and in the latter case, the change in C positions with respect to V_2C_2 is caused by the change in the divacancy configuration, i.e., V_2 prefers to be first or second nearest neighbor in clusters with or without He, respectively. In view of the lowest-energy configurations shown in Fig. 2, we note that the formation of a C dimer with strong covalent bond also contributes to stabilize clusters containing He.[14]

Binding energies corresponding to $He_{n-1}V_mC_p+He_{int} \rightarrow He_nV_mC_p$ and $He_nV_mC_{p-1}+C_{int} \rightarrow He_nV_mC_p$ reactions are detailed in Table I, where positive value means attraction. We note that C_{int}-to-complex binding energies are always lower than He_{int}-to-complex interaction energies, which is consistent with the fact that C-*V* interaction is much weaker than He_{int}-*V* interaction, being 0.41 and 2.30 eV the respective binding energies. He_{int}-to-complex binding energy is mainly dictated by the cluster pressure,[21,23,24] therefore it mostly decreases with increasing number of C in $He_nV_mC_p$ for given *n* and *m*. Carbon binding behavior is less simple. Binding energy of the first C atom to He_nV_m is also dictated by the cluster pressure, i.e., decreases with increasing number of He atoms at a given *m*. However, the energy gain associated to the inclusion of a second C into a cluster may be configuration dependent and depends rather on the strength of C-C bond formed in the resulting cluster, e.g., the C-to-HeV_2C binding energy is particularly high, 0.17 eV higher than that of C-to-V_2C binding. This is due to the difference in C and *V* positions between the respective resulting complexes: HeV_2C_2 and V_2C_2 [Figs. 2(f) and 1(h)]. The C_2 configuration in HeV_2C_2 is very close to that in VC_2 [Fig. 1(f)] where the addition of the second C induces the formation of a strong C-C covalent bond.[14] Indeed, the calculated C_2 bond length in both HeV_2C_2 and VC_2 are identical to that in graphene (1.42 Å) while the C_2 in V_2C_2 has a bond length of 1.04 Å, even shorter than that in an isolated C_2 dimer. The associated energy gain for VC_2 (0.77 eV) is clearly larger than that for V_2C_2 (0.68 eV) (Table I).

TABLE I. Binding energies of a He interstitial and a C atom to $He_{n-1}V_mC_p$ and $He_nV_mC_{p-1}$ complexes, respectively. The resulting clusters are listed in columns 1 and 4. All the energies are in electron volts.

	He_i	C		He_i	C
*V*C	—	0.41	V_2C	—	0.63
VC_2	—	0.77	V_2C_2	—	0.68
He*V*	2.30	—	HeV_2	2.78	—
He*V*C	2.03	0.14	HeV_2C	2.70	0.55
HeVC_2	1.44	0.18	HeV_2C_2	2.87	0.85
He_2V	1.84	—	He_2V_2	2.67	—
He_2VC	1.73	0.03	He_2V_2C	2.45	0.33
He_2VC_2	1.81	0.26	$He_2V_2C_2$	2.05	0.45

2. *Stability of small* $He_nV_mC_p$ *complexes*

In order to understand the impact of carbon on the thermal emission of He into He interstitial from He-vacancy-carbon clusters from the point of view of energetics, we have compared the stabilities of He_nV_m and $He_nV_mC_p$ complexes. The dissociation energies can be reasonably assumed to be the sum of the corresponding defect-complex binding energy and the migration energy of the isolated defect,[21,23,24] where the calculated migration energies for a vacancy, an interstitial He, or a C atom are, respectively, 0.67, 0.06, and 0.87 eV.[7,14,21] The obtained dissociation energies are shown in Fig. 3.

As mentioned in previous works,[7,24] the emission of a He into He interstitial from a He_nV_m complex requires lower energy barrier than the emission of a vacancy when the helium-to-vacancy ratio (n/m), i.e., cluster pressure, is high. The present results suggest a similar trend when these complexes contain C. The solute-from-complex dissociation is indeed energetically more favorable than the vacancy dissociation from HeVC_p and He_2VC_p complexes. Moreover, vacancy-from-$He_nV_mC_p$ dissociation energy increases systematically with $p=0-2$ while the one of He-from-$He_nV_mC_p$ rather decreases with *p* for given values of *n* and *m*. The emission of C from these ternary clusters is always more favorable than the emission of a He interstitial, which is

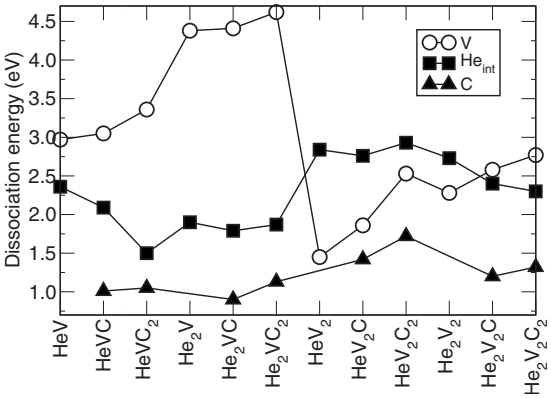

FIG. 3. Dissociation energies of a vacancy, a He atom or a C atom from a $He_nV_mC_p$ complex. The composition of the original clusters are shown in the abscise.

consistent with their respective binding energies. However, it is worth mentioning that the difference in their dissociation energies is relatively small in the case of $HeVC_2$ (0.45 eV). The origin of this fact is twofold: on one hand, the He atom is weakly bound in this complex due to increase in cluster pressure (Table I) induced particularly by the presence of C atoms. The $HeVC_2 \rightarrow He_{int} + VC_2$ reaction only costs 1.50 eV, i.e., 0.86 eV less than the substitutional He (He*V*) dissociation energy. On the other hand, C atoms are stabilized in the complexes due to the presence of C-C covalent bond[14] as already mentioned in the previous Subsection. The dissociation energy of C is therefore systematically higher from a $He_nV_mC_2$ than from a He_nV_mC complex with given values of n and m.

III. KINETICS OF HE-*V*-C CLUSTERS IN IRRADIATED FE

In this section we enumerate the various atomistic mechanisms describing the kinetics of helium, point defects, and point defect clusters in iron containing carbon. It is important to note that, in contrast to our previous work,[17] the formation of He-*V*-C complexes is explicitly taken into account in the present study. The mobile species considered here are monointerstitials and diinterstitials, monovacancies, interstitial helium, and interstitial carbon atoms. For simplicity, larger self-interstitial and vacancy clusters are considered immobile as in Ref. 17. Based on these assumptions, the reactions that govern the evolution of helium, carbon, point defects, and defect clusters in iron are the following: kick-out (KO) or replacement mechanism for helium

$$HeV + I \rightleftharpoons He_{int}, \tag{1}$$

where He*V* denotes a helium atom at substitutional site and I is a self-interstitial. Following this mechanism, a helium atom located at a substitutional site becomes mobile, i.e., jumps to an interstitial site, when is kicked out by a self-interstitial. This mechanism is expected to play an important role under irradiation conditions in which self-interstitials are generated in large amounts. Frank-Turnbull (FT) or dissociative mechanism for helium

$$HeV \rightleftharpoons He_{int} + V. \tag{2}$$

According to this reaction, a helium atom becomes mobile when a substitutional helium dissociates into a vacancy and an interstitial helium. Kick-out-like mechanism for carbon

$$VC + I \rightleftharpoons C_{int}. \tag{3}$$

The reaction above shows that a carbon atom trapped in a *V*C complex becomes mobile interstitial, C_{int}, when a self-interstitial recombines with the vacancy in the *V*C complex. Frank-Turnbull mechanism for carbon

$$VC \rightleftharpoons C_{int} + V. \tag{4}$$

This dissociative mechanism is similar to reaction (2) for helium. Formation of He-*V*-C clusters

$$He_nV_mC_p + He_{int} \rightleftharpoons He_{n+1}V_mC_p, \tag{5}$$

$$He_nV_mC_p + V \rightleftharpoons He_nV_{m+1}C_p, \tag{6}$$

$$He_nV_mC_p + C_{int} \rightleftharpoons He_nV_mC_{p+1}. \tag{7}$$

The atomic structures of these clusters were described in Sec. II. Recombination between self-interstitials and vacancies

$$I + V \rightleftharpoons 0. \tag{8}$$

Formation of self-interstitial clusters

$$I_n + I \rightleftharpoons I_{n+1}, \tag{9}$$

$$I_n + I_2 \rightleftharpoons I_{n+2} \tag{10}$$

in which I_n denotes clusters containing n self-interstitials. According to reactions (9) and (10), interstitial clusters can form by agglomeration of mobile self-interstitials and di-interstitials. Recombination of vacancies with self-interstitial clusters

$$I_n + V \rightarrow I_{n-1}. \tag{11}$$

The above reaction is considered to be irreversible due to its high binding energy. Recombination of self-interstitials with He-*V*-C clusters

$$He_nV_mC_p + I \rightarrow He_nV_{m-1}C_p. \tag{12}$$

The emission of a self-interstitial from a He-*V*-C cluster is neglected because of the high binding energy involved in the reaction, similar to the previous case. Although *ab initio* calculations[21] show that He can also diffuse in Fe by the migration of HeV_2 complexes, this mechanism was not included in this model. Indeed, the migration energy involved in this mechanism is relatively high (1.1 eV). Additional kinetic Monte Carlo simulations (not shown) performed in the case of pure Fe confirmed that this mechanism plays a minor role in the diffusion of He in the conditions that will be discussed here. Also, the interaction between either He_{int} or C_{int} with self-interstitial atoms are neglected in this study since the corresponding binding energies are significantly lower than those between He_{int} or C with vacancies.[9,23]

The atomistic processes considered in this model and presented above were described within a rate equation formal-

ism. In this formalism, it is assumed that reaction rates follow the kinetic law of mass action derived by Brönsted.[25] Then, according to the mass conservation, the time evolution of the concentration of mobile defects and immobile clusters is governed by a set of coupled nonlinear partial differential equations and ordinary differential equations. In practice, this leads for mobile defects to a set of one-dimensional spatial diffusion-reaction equations that are obtained by taking into account their diffusion and the generation-recombination terms corresponding to all possible reactions in which the mobile defects are involved, as done in a previous work.[8] On the other hand, when defects are immobile, such as $He_nV_mC_q$ and I_n clusters, they clearly follow a Markovian chain process and their kinetics can then be described by a master equation, as is done in Ref. 8. The reaction-rate constants corresponding to the reactions of the model were calculated following the methodology used in Ref. 8 and using the binding and migration energies of defects obtained by *ab initio* calculations. The binding energies of He-*V* clusters and migration energies of mobile defects were obtained previously by *ab initio* calculations.[7,21] The energetic properties of He-*V*-C clusters are presented in Sec. II of the present paper. As in our previous work,[17] migration energies of 0.06, 0.67, 0.34, and 0.42 eV for He_{int}, V, I, and I_2, respectively, were used in this model. Regarding the mobility of I_2 clusters, we are aware that recent calculations,[26] combining molecular dynamics and DFT methods, have revealed the existence of unexpected configurations of self-interstitial clusters in iron, formed by nonparallel ⟨110⟩ dumbbells. These calculations show that these new configurations are expected to have a somewhat lower mobility in comparison to previous atomistic simulations for *conventional* self-interstitial clusters. Thus, the migration energy of I_2 clusters should, in principle, be slightly larger than the one used in the current work. However, since I_2 clusters mainly play a role in the early formation of self-interstitial clusters, we believe that the results obtained here should not change with the migration energy of I_2. In order to account for the recombination and/or out diffusion of defects at the surface, first-order boundary conditions were used, assuming that the flux of defects at the surface is proportional to the excess of defects at the surface and only limited by diffusion, as done in Ref. 8. However, in the case of interstitial carbon, we assumed the flux at the surface to be null since there is no physical evidence according to which carbon could escape from the surface. The rate equations corresponding to reactions (1)–(12) together with the different boundary conditions were solved using the partial differential equation solver PROMIS 1.5.[27]

IV. MECHANISMS OF HE DESORPTION IN FE CONTAINING CARBON

The aim of this section is to evidence the role of carbon and to determine the dominant mechanisms that govern He desorption in irradiated Fe containing carbon. As a good approximation, we only included explicitly in the RT model a minimal set of defect clusters which was necessary to capture the main features of the mechanisms described in Sec III, that is, He_nV_m with $n=0-4$ and m unlimited such as in Ref. 17, and $He_nV_mC_p$ complexes (n, m, and $p=0-2$). The binding energies of He_nV_m clusters with (n and $m=0-4$) were obtained by *ab initio* calculations.[21] For He_nV_m clusters with $m \geq 4$, an extrapolation law was used to calculate the binding energies, as done in other works.[7,28] We have simulated He desorption in Fe during isothermal annealings for various He concentrations, temperatures, and for carbon concentrations ranging from 5 to 200 at.ppm. In all cases we considered the initial He concentration as homogeneous over the thickness of the sample. All simulations presented here were performed for a sample thickness of 20 μm. An initial point-defect concentration of 200 Frenkel pairs (*I*-*V*) per implanted He was used, which fairly corresponds to conditions reached under high-energy He irradiation according to TRIM (transport of ions in matter) (Ref. 29) simulations.[17] We are aware that more accurate damage results could be obtained with other methods, e.g., with molecular-dynamics simulations, which would provide a more accurate damage distribution. However, for the case of light ions such as He, binary collision models with the proper displacement threshold energy for Frenkel pair production −40 eV in the case of Fe—are a good approximation.

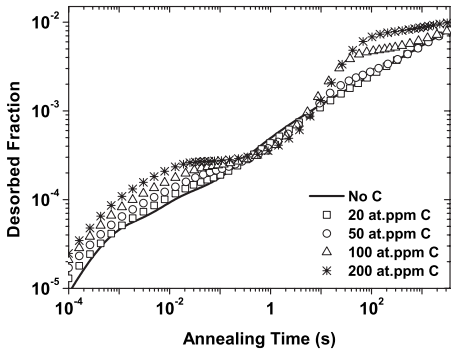

FIG. 4. Evolution of the desorbed fraction of He during an isothermal annealing at 573 K for an initial He concentration of 0.1 at.ppm and for various carbon concentrations.

Considering the defects present after irradiation, i.e., He_{int}, I, and V, and carbon staying initially at interstitial sites, the evolution of the system at room temperature (300 K) is simulated until quasi-steady state is reached, i.e., a state that does not evolve significantly at macroscopic time scales. Indeed, interstitial atoms (I and He_{int}) are highly mobile and can migrate even at low temperature.[7,21] Then, the He desorption is simulated during isothermal annealing at temperature T.

A. Low He content

In Fig. 4 we reported the simulated He desorption curves obtained at $T=573$ K for an initial He concentration of 0.1 at.ppm and for carbon concentrations ranging from 20 to 200 at.ppm. For comparison, the desorption curve simulated in pure Fe is also included. As clearly shown in Fig. 4, our model predicts that He desorption is significantly affected by carbon impurities for carbon concentrations higher than 50 at.ppm, in comparison to the case where He diffuses in pure Fe. In particular, we can see that He desorption is enhanced,

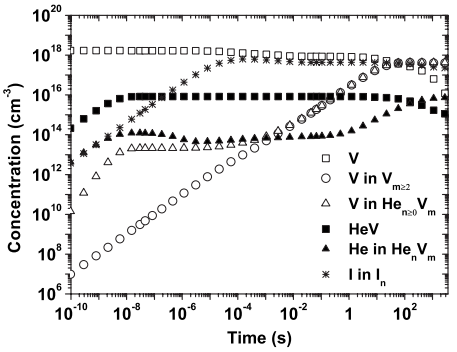

FIG. 5. Evolution of main species at room temperature (300 K) in pure Fe (without carbon) after He irradiation for an initial He concentration of 0.1 at.ppm.

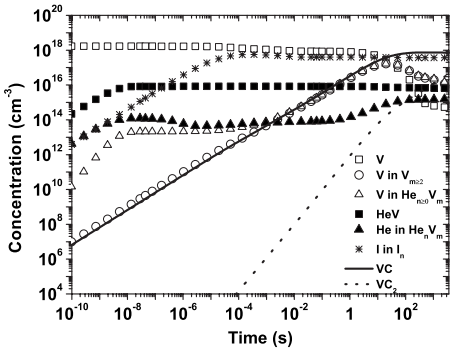

FIG. 6. Evolution of main species at room temperature (300 K) in Fe containing 200 at.ppm of carbon after He irradiation and for an initial He concentration of 0.1 at.ppm.

at least in the conditions of temperature and in the time range considered here. Furthermore, distinct desorption regimes emerge at high carbon concentrations, suggesting that more than one thermally activated mechanism govern desorption. The effect gets more pronounced as the carbon concentration increases, though it seems to saturate at high concentrations. At high carbon concentrations, our model predicts an ultrafast desorption at the early stages of annealing, followed by a plateau, indicating first a fast release of He followed by a strong reduction in the formation of mobile helium atoms. This plateau is then followed by a rapid He release and a slower rate at later times. Clearly, the atomistic processes that control He diffusion and clustering in Fe containing carbon are different than those that prevail in pure Fe, at least for carbon concentrations higher than 50 at.ppm. Notice that a clear influence of carbon can be seen on He desorption when the V/C ratio is low, i.e., for carbon concentrations higher than the vacancy concentration (20 at.ppm here).

In order to determine how carbon affects He desorption in the case of a low He content, we shall first examine the different species that form at room temperature in the two extreme cases: pure Fe and Fe containing 200 at.ppm of carbon.

Figure 5 shows the evolution of the main species that form at 300 K after He irradiation in pure Fe. The quantities showed in this figure represent the concentrations averaged over the depth. This figure evidences that most of interstitial helium atoms, which migrate rapidly at room temperature, jump into substitutional sites in a very short time ($\sim 10^{-8}$ s) by recombination with vacancies following the reaction $\mathrm{He}_{\mathrm{int}}+V\rightarrow \mathrm{He}V$. Vacancies are also mobile at room temperature and after an approximate time of 100 s, most vacancies are agglomerated into clusters that do not contain helium, as can be seen by comparing the evolution of V in $V_{m\geq 2}$ (open circles) and the one of V in He_nV_m clusters (open triangles: includes all He-V clusters except V and HeV). On the other hand, simulations show that a small fraction of mobile vacancies also reacts with substitutional HeV and form, by successive reactions, $\mathrm{He}V_2$, $\mathrm{He}V_3$, and $\mathrm{He}V_4$ clusters. As a consequence, the number of substitutional He (HeV) formed at the early stages of the annealing decreases (full squares) and the number of helium atoms trapped in immobile clusters He_nV_m (full triangles: excludes HeV) increases accordingly. We can see that at 300 K most self-interstitials generated during irradiation diffuse and agglomerate into small $I_{n\geq 2}$ clusters after a short time of about 10^{-4} s. This is not surprising since self-interstitials have a low migration energy (0.34 eV) and interstitial clusters exhibit a relatively high binding energy. In summary, our model predicts that after He irradiation in pure Fe at room temperature (300 K), helium is expected to be mainly found in small $\mathrm{He}V_{m\geq 2}$ complexes and a small proportion at substitutional sites (HeV). On the other hand, most vacancies and self-interstitials generated during irradiation are expected to agglomerate into small vacancy clusters $V_{m\geq 2}$ and small interstitial clusters $I_{n\geq 2}$, respectively.

When He is implanted in Fe containing carbon, our model predicts a situation significantly different at 300 K than in the case of pure Fe. In order to clearly illustrate this, in Fig. 6 we reported the evolution of the main species that form after irradiation at 300 K, for the highest carbon concentration (200 at.ppm). As in the previous situation, simulations predict that a large amount of interstitial helium atoms incorporates into substitutional sites by recombination with vacancies in a very short time. Figure 6 evidences that most of the implanted He atoms can be found at substitutional sites (full squares) after a time of about 10^{-8} s. As one can see, after a time of about 10 s, most vacancies generated during irradiation are trapped into VC complexes. We can also see that a small amount of vacancies are trapped into $V\mathrm{C}_2$ clusters. Simulations indicate that these complexes form following $V\mathrm{C}+\mathrm{C}_{\mathrm{int}}\rightarrow V\mathrm{C}_2$ and $\mathrm{C}_2+V\rightarrow V\mathrm{C}_2$. Note that although $\mathrm{C}_{\mathrm{int}}$ atoms are barely mobile at room temperature, they are present in high concentration, which increases the probability of these latter reactions. Hence, in contrast to the case of pure Fe, the agglomeration of vacancies into V_m clusters is strongly inhibited when carbon is present in high concentration. Note that in that case, the concentration of carbon is significantly higher than the concentration of vacancies. Simulations also show that at 300 K a small fraction of helium can be found in small immobile He-vacancy clusters. These clusters are mainly $\mathrm{He}V_2$, the formation of other $\mathrm{He}V_{m>2}$ clusters being significantly reduced, in contrast to the case of pure Fe. This can be easily explained by the fact that in this case, vacancies created during irradiation are mainly trapped by carbon atoms in VC and $V\mathrm{C}_2$ complexes,

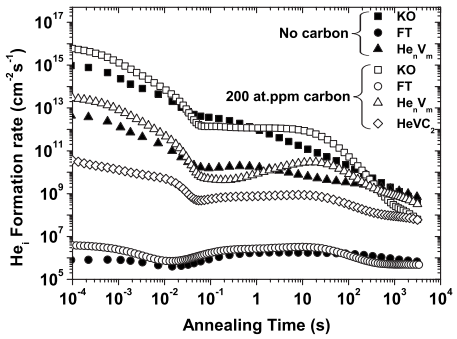

FIG. 7. Formation rates of He_{int} from different reactions for a 573 K isothermal annealing calculated after the steady state reached at 300 K after an He irradiation with an initial He concentration of 0.1 at.ppm; without carbon (full symbols) and with carbon (open symbols).

as seen in Fig. 6. This trapping strongly reduces the number of free vacancies and thus inhibits reactions of the type $HeV_m+V \rightarrow HeV_{m+1}$. As in the case of pure Fe, most of self-interstitials generated during irradiation quickly agglomerate into I_n clusters at room temperature. It is worth noticing that in this case, the number of self-interstitials agglomerated in clusters is slightly higher than in the case where carbon is absent. Again, this can be explained by the large amount of vacancies that are trapped by carbon atoms at room temperature, which reduces the number of I-V and/or I_n-V recombinations. Thus, the main defects that form at room temperature in Fe containing 200 at.ppm of carbon and irradiated with He are HeV, VC, and I_n. Our model also predicts the formation of small vacancy clusters, HeV_2 and VC_2 clusters but in relatively small concentration.

Having identified the species that form at room temperature after He irradiation in pure Fe and Fe containing a high concentration of carbon, we shall now determine and compare the atomistic mechanisms that govern He desorption during a subsequent isothermal annealing in Fe with and without carbon. To do so, we monitor the temporal evolution of the formation rates of He_{int}. Indeed, mobile helium atoms (He_{int}) must form and reach the surface prior He desorption occurs. According to the model presented here, a mobile He_{int} can form by the KO mechanism ($HeV+I \rightarrow He_{int}$), by the FT mechanism, i.e., dissociation of a substitutional He ($HeV \rightarrow He_{int}+V$) and by dissociation from He_nV_m and $He_nV_mC_p$ clusters. In the rest of the manuscript, dissociation from He_nV_m clusters means dissociation from all Helium-vacancy clusters except the particular case of HeV. The He_{int} formation rates corresponding to these reactions and for $T=573$ K are reported in Fig. 7 for the case of pure Fe and for the highest carbon concentration considered here (200 at.ppm) for an initial He concentration of 0.1 at.ppm. The rates reported in this figure were obtained by integration of the rates of the different reactions over the depth of the sample.

In the case of pure Fe (full symbols), we can see that the formation of mobile helium during annealing at 573 K is mainly due, at least in this time range, to the KO mechanism. This clearly indicates that self-interstitial clusters I_n formed at room-temperature dissociate during the isothermal annealing, releasing a large flux of self-interstitials that kick the substitutional helium atoms—formed at 300 K as well—out of their sites. As it was already concluded in our previous work,[17] self-interstitial clusters that form at low temperature right after irradiation still play an important role in He diffusion during subsequent annealing and cannot be neglected. For annealing times longer than 1000 s the contribution of the dissociation of He from He_nV_m clusters to the desorption starts being comparable to that of the KO mechanism. The contribution of the dissociation of HeV is always much lower than either of these other two mechanisms. This is due to the relatively high dissociation energy (2.30 eV) of the reaction $HeV \rightarrow He_{int}+V$.

In the case of Fe containing 200 at.ppm of carbon, Fig. 7 shows that the formation of mobile helium at the early stages of annealing is also due to the KO mechanism, as expected. However, we can see that in this case, at the beginning of annealing the rate of He_{int} formation due to the KO mechanism is higher than the one expected in pure Fe, by about 1 order of magnitude. Undoubtedly, the desorption enhancement predicted to occur at the early stages of annealing for a carbon concentration of 200 at.ppm (see Fig. 4) corresponds to this ultrafast release of He due to KO at short times ($t \lesssim 10^{-2}$ s). On one hand, the increase in the rate of reactions $HeV+I \rightarrow He_{int}$ can be explained by the fact that the concentration of HeV complexes that form at room temperature is significantly larger when carbon is present in Fe than in pure Fe, as can be seen by comparing Figs. 5 and 6. Thus, when interstitial clusters dissolve, self-interstitials that are emitted *see* more HeV atoms, resulting in a larger rate of KO reactions. As explained before, the concentration of substitutional He atoms significantly increases at room temperature when carbon is present due to the large amount of vacancies that are trapped by carbon into VC and VC_2 complexes, which strongly inhibits reactions between vacancies and HeV atoms. A detailed analysis of simulation results reveal (not shown) that this increase in the rate of KO reactions also results from a larger emission rate of self-interstitials from I_n clusters—formed at room temperature—when they start dissolving at the early stages of the isothermal annealing. This higher I flux is due to the larger number of self-interstitials that agglomerate into I_n clusters at room temperature due to the trapping of vacancies by carbon as explained before. Thus, the enhancement of He desorption expected at short times for a low He content and in the presence of a high carbon concentration is primarily due to the high concentration of VC and VC_2 complexes that form at room temperature. It is important to note that most vacancies trapped into VC clusters at room temperature do not dissociate during the isothermal annealing at 573 K but remain trapped into carbon complexes. Indeed, Fig. 8 evidences that at the early stages of the annealing at 573 K ($\sim 10^{-3}-10^{-2}$ s), VC complexes transform into VC_2 complexes following the reaction $VC+C_{int} \rightarrow VC_2$. These latter are stable at this temperature and only start dissociating at a time of about 10^2 s, as can be seen in Fig. 8. The rest of the vacancies—a small fraction—is mainly found in small He_nV_m clusters containing at least one He atom. A smaller proportion of vacancies are agglomerated into small $V_{m \geq 2}$. Carbon seems thus to be an efficient trap for vacancies and significantly affects their migration at room temperature and up to, at least, a temperature of 573 K.

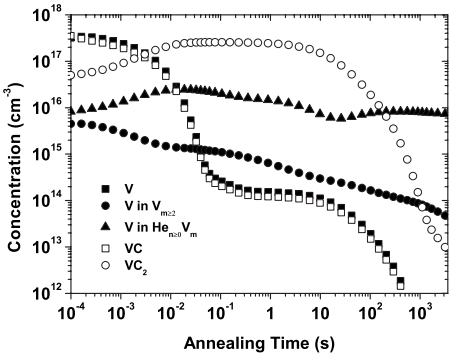

FIG. 8. Evolution of vacancy species at 573 K in Fe containing 200 at.ppm of carbon after the steady state reached at 300 K after an He irradiation with an initial He concentration of 0.1 at.ppm.

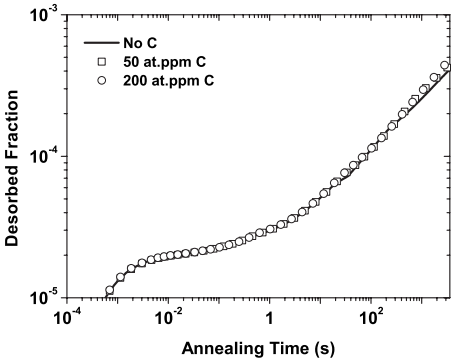

FIG. 9. Evolution of the desorbed fraction of He during an isothermal annealing at 573 K for an initial He concentration of 10 at.ppm and for carbon concentrations of 50 and 200 at.ppm.

After the period of ultrafast release of helium, the He_{int} flux from the KO mechanism is reduced by almost 4 orders of magnitude in a short time, which explains the slow desorption regime—the plateau—seen after $t \simeq 10^{-2}$ s in the desorption curve corresponding to a carbon concentration of 200 at.ppm. Simulation indicate that this occurs when small I_n clusters have dissolved and only large interstitial clusters—which are more stable—are left and thus, dissolve at a much slower rate. This stage clearly appears at high carbon concentration due to the significant reduction in recombinations $I_n + V \rightarrow I_{n-1}$, which allows I_n clusters to grow toward larger sizes, i.e., more stable configurations. This occurs as a result of the trapping of most vacancies by carbon into VC and VC_2 complexes, as explained before.

As we can see, for intermediate times (between 1 and 100 s) the formation of He_{int} is still mainly due to KO reactions, according to Fig. 7. This phase corresponds to the slow dissolution of large I_n clusters. During this interval, the resulting formation rate of He_{int} is more or less constant and higher than the one expected in pure Fe, which results in the desorption enhancement, in comparison to desorption from pure Fe, as seen in Fig. 4 at intermediate times.

Figure 7 shows that for long annealing times, the He_{int} flux due to the KO continuously decreases due to the final dissolution of interstitial clusters. The formation of mobile He_{int} and thus He desorption is then governed by several mechanisms at the same time, namely, the KO mechanism, the dissociation from He_nV_m clusters, and the dissociation from $HeVC_2$ complexes. Simulations reveal that various reactions are necessary for these latter complexes to form. When interstitial carbon becomes mobile it interacts with substitutional helium atoms formed at room temperature leading to the formation of $HeVC$ clusters. At the same time they form, $HeVC$ clusters react with other interstitial carbon atoms, thus forming $HeVC_2$ complexes. The total formation rate of mobile He_{int} resulting from the different mechanisms is relatively low and corresponds to the slow desorption rate seen at later times in Fig. 4. It is worth to note that in both cases—pure Fe and Fe with carbon—the contribution of the dissociative mechanism ($HeV \rightarrow He_{int} + V$) to the desorption of He is much smaller than the contribution of the other mechanisms.

B. High He content

In Sec. IV A we studied the effect of carbon on He kinetics in Fe in the case of a low He content, namely, 0.1 at.ppm. In Sec. IV B we shall study He desorption in the case where the concentration of He is two orders of magnitude higher and for different carbon concentrations, as in the case above. Figure 9 shows the desorption curves calculated for an initial He concentration of 10 at.ppm and for a maximum carbon concentrations of 200 at.ppm. As before, we consider that there is 200 I-V pairs created per implanted He. In these conditions there is thus initially a vacancy concentration of 2000 at.ppm for a maximum carbon concentration of 200 at.ppm, that is, we are always in a situation of high V/C ratio. Figure 9 clearly evidences that in these conditions, at least for the helium and carbon concentrations considered here, there is no influence of carbon on He desorption. In light of what was explained in Sec. IV A, the results obtained for a high V/C ratio can be easily explained. In Fig. 10 we compare the evolution of the main vacancy species that form at room temperature in the case of pure Fe and Fe containing 200 at.ppm of carbon. We can see that in both cases the evolution of free V and agglomerated V into $V_{m\geq 2}$ is the same, which clearly indicates that carbon barely affects vacancy migration, in contrast to what is expected for a low V/C ratio (see Sec. IV A). Only a small fraction of vacancies initially created are trapped into carbon complexes. This is

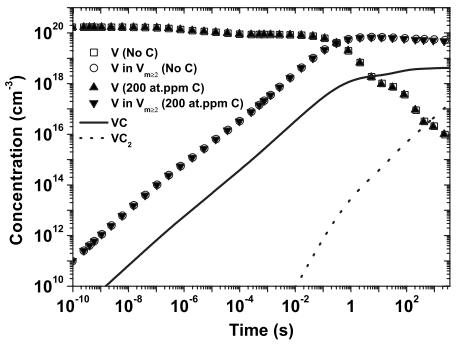

FIG. 10. Evolution of vacancy species at room temperature (300 K) in pure Fe and in Fe containing 200 at.ppm of carbon for an initial He concentration of 10 at.ppm.

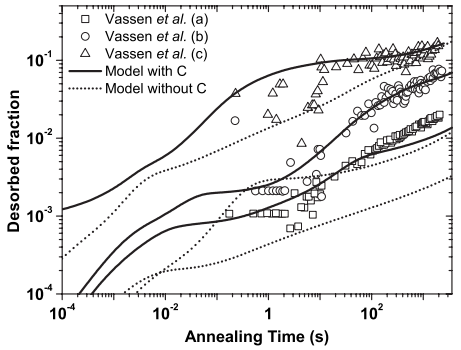

FIG. 11. Comparison between experimental He desorbed fraction obtained by Vassen *et al.* (Ref. 18) in conditions (a), (b), and (c) (see text), our previous model without carbon (dotted lines) and our model including formation of He-*V*-C complexes (continuous lines).

expected since in this case the initial amount of vacancies is much larger than the amount of carbon. Thus, our model predicts that the effect of carbon on He desorption is negligible for a high V/C ratio since only a small fraction of vacancies are trapped into carbon complexes.

V. COMPARISON MODELING VERSUS HE DESORPTION EXPERIMENTS

We used the model described above to reproduce the desorption experiments that were carried out by Vassen *et al.*[18] In these experiments the authors studied the thermal desorption of high-energy helium homogeneously implanted in iron. To obtain basic information about He diffusion mechanisms in α-Fe, the authors measured the released fraction of helium during isothermal annealing for various temperatures, foil thicknesses, and initial He concentrations: (a) 559 K, 2.5 μm, 1.39 at.ppm, (b) 577 K, 20.6 μm, 0.013 at.ppm, and (c) 667 K, 2.6 μm, 0.109 at.ppm. The irradiation conditions used here are those used in Sec. IV, that is, 200 *I-V* pairs per implanted He. As in Sec. IV B, considering the defects generated by the irradiation process—He_{int}, *I*, and *V*—and also carbon atoms initially at interstitial sites, we simulated the evolution of the system at room temperature (300 K) until the system does not evolve significantly at macroscopic time scales. Then, after the 300 K calculation, He desorption during isothermal annealing was simulated for the experimental conditions described in Ref. 18. At this point we want to emphasize that the only free parameter of our model is the carbon concentration present in the samples, which is a characteristic of the material that has not been specified. This parameter was then modified until a good agreement with experimental desorption data was reached for each condition described above. This was obtained for a carbon concentration of about 150 at.ppm for the different conditions, which seems in agreement with the nominal purities of samples given in Ref. 18. Results obtained with the model without carbon[17] are reported for comparison. As shown in Fig. 11, with this value for the carbon concentration the model reproduces very well the different experimental phases of He desorption over several orders of magnitude in time and for very different conditions of temperature, sample thickness, and He concentration. This result clearly demonstrates the importance of carbon in the kinetics of He in Fe. This result also clearly evidences that any investigation on the void swelling phenomenon in metals under irradiation should not only focus on the formation of He-*V* complexes but should also consider possible interactions between vacancies and/or helium with impurities that are always present in samples, in particular in industrial stainless steels intended for the construction of nuclear power plants.

The mechanisms involving carbon described in Sec. III and the carbon concentration extracted from experimental data allow us to understand the anomalous migration energy of vacancies we found in our previous work.[17] Indeed, using a model not including carbon interactions, we found that an effective vacancy migration energy of 0.83 ± 0.8 eV was necessary to obtain a good agreement with experimental He desorption data, instead of the theoretical value 0.67 eV found by DFT calculations. This high value was explained by invoking the interaction between vacancies and impurities in experimental samples, which was not explicitly taken into account in our model. The present investigation confirms this assumption and explains the high migration energy of vacancies—slower diffusion—found in our previous work as the result of the trapping of vacancies by carbon into *V*C and VC_2 complexes.

VI. CONCLUSIONS

In this work density functional theory calculations were performed to study the interaction of carbon with He-vacancy complexes in α-Fe. We show that the formation of small He-*V*-C complexes is indeed energetically favorable. The lowest-energy configurations of $He_nV_mC_p$ clusters with n, m, and $p=0-2$ have been investigated. He atoms are found to stay at off-site positions, as far as possible from the C atoms due to their mutual repulsion. On the other hand, C atoms remain as close as possible to octahedral interstitial sites and the formation of covalent C-C bonds contributes to stabilize clusters both with and without He atoms. Calculations show that the dissociation of these ternary clusters via emission of a C atom always implies a lower energy than the emission of a He interstitial, the energy difference being minimal for the $HeVC_2$ complex.

A rate theory model based on the results obtained by DFT calculations and accounting for interactions between helium, defects created during irradiation and carbon, was then developed to investigate the mechanisms of He desorption in irradiated α-Fe containing carbon. Results obtained with this kinetic model evidence a clear influence of carbon on He desorption when the V/C ratio is low ($\lesssim 0.2$). In this case our model predicts a significant influence of carbon on He desorption with increasing carbon concentrations. A detailed analysis showed that this effect is mainly due to the trapping at room temperature of a large amount of vacancies into *V*C and VC_2 clusters rather than the formation of He-*V*-C complexes. For a high V/C ratio ($\gtrsim 10$), our study predicts that carbon barely influences He desorption. Calculations showed that in this case, only a small fraction of vacancies generated

during irradiation are trapped by carbon, which does not affect He kinetics. Our *ab initio* based rate theory model including carbon was then used to reproduce experimental He desorption reported in the literature. With the parameters determined from first principles our model including carbon was able to reproduce successfully the different experimental phases of He desorption in irradiated α-Fe over a wide range of time and temperature. Further experiments on very high-purity samples with well-controlled carbon concentrations would contribute validation of the model presented here. Finally, this work clearly evidences that any investigation on the void swelling phenomenon in metals under irradiation should not only focus on the properties of He-V complexes but should also consider possible interactions between vacancies and/or helium with impurities that are always present in experimental samples.

ACKNOWLEDGMENT

This work was funded by the European fusion materials modeling program. Part of this work was performed using HPC resources from GENCI-CINS (Grant 2009-x2009096020).

*Email address: christophe.ortiz@ciemat.es
†Email address: chuchun.fu@cea.fr

[1] E. E. Bloom, J. T. Busby, C. E. Duty, P. J. Maziasz, T. E. McGreevy, B. E. Nelson, B. A. Pint, P. F. Tortorelli, and S. J. Zinkle, J. Nucl. Mater. **367-370**, 1 (2007).
[2] R. Andreani, E. Diegele, R. Laesser, and B. van der Schaaf, J. Nucl. Mater. **329-333**, 20 (2004).
[3] N. Baluc, R. Schaublin, P. Spatig, and M. Victoria, Nucl. Fusion **44**, 56 (2004).
[4] C. Domain and C. S. Becquart, Phys. Rev. B **65**, 024103 (2001).
[5] C. C. Fu, F. Willaime, and P. Ordejón, Phys. Rev. Lett. **92**, 175503 (2004).
[6] D. Nguyen-Manh, A. P. Horsfield, and S. L. Dudarev, Phys. Rev. B **73**, 020101(R) (2006).
[7] C. C. Fu, J. Dalla Torre, F. Willaime, J.-L. Bocquet, and A. Barbu, Nature Mater. **4**, 68 (2005).
[8] C. J. Ortiz and M. J. Caturla, Phys. Rev. B **75**, 184101 (2007).
[9] S. Takaki, J. Fuss, H. K. U. Dedek, and H. Schultz, Radiat. Eff. **79**, 87 (1983).
[10] A. Vehanen, P. Hautojarvi, J. Johansson, J. Yli-Kauppila, and P. Moser, Phys. Rev. B **25**, 762 (1982).
[11] A. Hardouin-Duparc and A. Barbu, Mater. Res. Soc. Symp. Proc. **439**, 509 (1997).
[12] M. Kiritani, Ultramicroscopy **39**, 135 (1991).
[13] C. Domain, C. S. Becquart, and J. Foct, Phys. Rev. B **69**, 144112 (2004).
[14] C. C. Fu, E. Meslin, A. Barbu, F. Willaime, and V. Oison, Solid State Phenom. **139**, 157 (2008).
[15] C. J. Först, J. Slycke, K. J. Van Vliet, and S. Yip, Phys. Rev. Lett. **96**, 175501 (2006).
[16] C. C. Fu and F. Willaime, C. R. Phys. **9**, 335 (2008).
[17] C. J. Ortiz, M. J. Caturla, C. C. Fu, and F. Willaime, Phys. Rev. B **75**, 100102(R) (2007).
[18] R. Vassen, H. Trinkaus, and P. Jung, Phys. Rev. B **44**, 4206 (1991).
[19] C. J. Ortiz, M. J. Caturla, C. C. Fu, and F. Willaime, J. Nucl. Mater. **386-388**, 33 (2009).
[20] J. M. Soler, E. Artacho, J. D. Gale, A. Garcia, J. Junquera, P. Ordejón, and D. Sanchez-Portal, J. Phys.: Condens. Matter **14**, 2745 (2002).
[21] C. C. Fu and F. Willaime, Phys. Rev. B **72**, 064117 (2005).
[22] T. Seletskaia, Y. Osetsky, R. E. Stoller, and G. M. Stocks, Phys. Rev. Lett. **94**, 046403 (2005).
[23] C. C. Fu and F. Willaime, J. Nucl. Mater. **367-370**, 244 (2007).
[24] K. Morishita, R. Sugano, B. D. Wirth, and T. Diaz de la Rubia, Nucl. Instrum. Methods Phys. Res. B **202**, 76 (2003).
[25] J. Bronsted, Z. Phys. Chem. **102**, 169 (1922).
[26] D. A. Terentyev, T. P. C. Klaver, P. Olsson, M.-C. Marinica, F. Willaime, C. Domain, and L. Malerba, Phys. Rev. Lett. **100**, 145503 (2008).
[27] P. Pichler, W. Jungling, S. Selberherr, E. Guerrero, and H. W. Pöltz, IEEE Trans. Comput.-Aided Des. **4**, 384 (1985).
[28] A. Hardouin-Duparc, C. Moingeon, N. Smetniansky-de-Grande, and A. Barbu, J. Nucl. Mater. **302**, 143 (2002).
[29] J. P. Biersack and L. G. Haggmark, Nucl. Instrum. Methods **174**, 257 (1980).